CRP-binding bacteriophage as a new element of layer-by-layer assembly carbon nanofiber modified electrodes

Katarzyna Szot-Karpińska [1*], Patryk Kudła [1], Anna Szarota [1],
Magdalena Narajczyk [2], Frank Marken [3], Joanna Niedziółka-Jönsson [1]

[1] *Institute of Physical Chemistry, Polish Academy of Sciences, Kasprzaka 44/52, 01-224 Warsaw, Poland*

[2] *Department of Electron Microscopy, Faculty of Biology, University of Gdansk, Wita Stwosza 59, 80-308 Gdansk, Poland*

[3] *Department of Chemistry, University of Bath, Bath BA2 7AY, United Kingdom*

[*] To whom correspondence should be addressed:

E-mail: kszot@ichf.edu.pl. Tel: +48 223433130, fax: +48 223433333

Abstract

Recently, bacteriophage particles have started to be applied as a new biomaterial for developing sensing platforms. They can be used as both a recognition element or/and as building blocks, template/scaffold. In this paper, we studied a bacteriophage selected through phage-display technology. The chosen bacteriophage acted as a building block for creating a carbon nanofiber-based electrode and as a new receptor/binding element that recognizes C-reactive protein (CRP) – one of the markers of inflammatory processes in the human body. The binding efficiency of the selected phage towards CRP is two orders of magnitude higher than in the wild type. We demonstrate that the phage-based sensor is selective against other proteins. Finally, we show that layer-by-layer methods are suitable for deposition of negatively charged phages (wild or CRP-binding) with positively charged carbon nanofibers for electrode surface modification. A three-layered electrode was successfully used for molecular recognition of CRP, and the molecular interactions were studied using electrochemical, biological, and optical methods, including microscopic and spectroscopic analyses.

Keywords: Bacteriophage; Phage-Display; Carbon nanofibers; Layer-by-Layer; Electrode modification; CRP detection

1. Introduction

Bacteriophages (phages, in short) are viruses of bacteria and are the most common biological entities on Earth. They are often used in molecular biology, where they serve as model particles. It was bacteriophages which led to the proof that DNA contains genetic information. Currently, they have found applications in environmental analysis as an indicator of water contamination, and medicine, for example, as an alternative to antibiotics (phage therapy) [1]. Moreover, phages can be engineered to express specific peptides, thus enabling researchers to modify their chemical properties considerably. Therefore, phages can be used to mimic existing biological molecules - for instance, antibodies [2–4]. The "phage-display" technique can be applied to generate such artificial antibodies [5]. G. Smith and G. Winter were awarded the Nobel Prize in chemistry in 2018 for developing this technique. The phage display is an incredible tool with ample opportunities for applications. Phages are non-pathogenic organisms for mammals and intrinsic entities of the human body, e.g., in the gut or the skin [6–8]. There are studies that have introduced the biopanning of phage libraries against eukaryotic cells [9]. Biopanning can be performed *in vivo* in mice as a model organism [10,11]. Work with phages does not require a high-level biosafety laboratory and is usually conducted in basic biosafety level 1 laboratory environments.

A relentless search for new applicable materials to be used in electrochemical sensors and electronic devices encourages scientists to turn towards interdisciplinary opportunities. In this aspect, the linkage of biology, chemistry, and material sciences is especially interesting. Phages – especially the filamentous M13 phage – are increasingly used in electrochemical applications as a template/scaffold for developing new materials [12–20] or as sensing elements for recognizing bacterial cells [21,22], cancer cells [23] or various disease markers [19,24,25].

C-reactive protein (CRP) is an annular pentameric protein found in blood plasma. An increased concentration of CRP in the blood (above 10 mg L^{-1}) is one of the markers indicative of a state of inflammation in the human body [26]. It is an acute-phase protein, and circulating concentrations rise rapidly and extensively in a cytokine-mediated response to tissue injury, infection, and inflammation processes. This increase follows secretion of interleukin-6 by macrophages and T cells. CRP is synthesized primarily in liver hepatocytes, but also in smooth muscle cells, macrophages, endothelial cells, lymphocytes, and adipocytes. It binds to lysophosphatidylcholine expressed on the surface of dead or dying cells to activate the complement system via C1q [27]. CRP occurs in two isoforms, native and monomeric CRP, termed nCRP and mCRP, respectively. The nCRP and mCRP forms are working in opposite manners. nCRM is involved in the inhibition of nitric oxide production, does not

influence the level of proinflammatory cytokine (IL-8, MCP-1), and has prominent anti-inflammatory activities [28]. Currently, both of these isoforms are being thoroughly investigated in inflammation and infection [28,29].

Generally, anti-nCRP antibodies [30] are used for CRP assays (anti-mCRP are not available [28]). However, also several so-called artificial antibodies like aptamers, with an assay range 0.005–125 ng mL^{-1} [31], affimers with detection range 0–1000 nM [32], polypeptide-conjugate binders (2–500 mg L^{-1}) [33] and molecularly imprinted polymers (10^{-12}–10^{-1} ng mL^{-1}) [27], have been used for molecular recognition of CRP. CRP is essential for monitoring and diagnosing various conditions such as cardiovascular, tumours, and autoimmune diseases [26]. Even though the main function of CRP is well-known in the literature, there is still a need to investigate its role in the body further. Recently, CRP was identified as one of the markers of rheumatoid arthritis [36].

Serum CRP values are routinely measured to detect and monitor many human diseases. While bacterial infection and active inflammation can increase of the CRP level of between 40–200 mg L^{-1} a smaller response (10–40 mg L^{-1}) is observed for viral infections and any mild inflammations. In the case of serious bacterial infections and burns, the CRP level can increase above 200 mg L^{-1} [37]. Therefore, CRP testing is essential for the differentiation between viral and bacterial infections, which is especially important with the advent of antimicrobial resistance [37].

According to the American Society of Microbiology, there is a constant need to develop innovative, rapid diagnostics that can quickly identify whether patients need antibiotics [38]. Generally, an evaluation of the CRP concentration in blood is performed using standard molecular diagnostic tools like automated immunotubindimetry or immunonephelometry with a detection range from 50 ng mL^{-1} to 10 μg mL^{-1}, and enzyme-linked immunoassay (ELISA) with an assay range to 100 ng mL^{-1} [39]. However, these techniques are expensive, laborious, and require skilled personnel. New CRP methods are being developed, which in contrast to the techniques mentioned above, can be cheaper, faster, easier to use, and can be miniaturized. These include such methods as chemiluminescence with detection range 0.3–3000 ng mL^{-1} [40], colorimetry (0.889–20.7 μg mL^{-1}) [41] electrochemistry (0–1000 nM, 5–220 fg mL^{-1}) [32,42], fluorescence (0.01–29 mg L^{-1}) [43], surface plasmon resonance (2–5 μg–mL^{-1}) [44], and lateral flow device detection (0.039–2.5 μg mL^{-1}) [45]. Commercially available CRP tests, which are based on antibodies, are expensive, which significantly limits their accessibility. Therefore, the approach of using phage particles and the phage-display method for the identification of new, cheaper CRP receptors could be a solution to improving the availability of CRP testing.

In this report, a new sensing element – a CRP-binding bacteriophage, generated via phage-display technology - is presented. An application in molecular recognition of CRP is demonstrated. The binding efficiency of the selected phage towards CRP is two orders of magnitude higher in comparison with the wild type. We also demonstrate the selectivity of the new phage against other proteins. We used a layer-by-layer (LbL) method for immobilization of the negatively charged phage (wild or CRP-binding) with positively charged carbon nanofibers on the electrode surface via electrostatic interactions. So far, only covalent binding was utilized for immobilization of the M13 phage on a substrate via LbL [46]. Electrochemical characterization of electrodes modified with the CRP-selective phage (P2-CRP) and the phage together with carbon nanofibers (P2-CRP/CNF) show that these electrodes are recognizing the CRP in the range from 4 to 40 μg mL^{-1}. The electrode modified with three layers of P2-CRP/CNF exhibited the best performance in the detection of CRP, making it a promising biosensing platform. The new CRP-binding phage obtained within our studies could become a long-sought-after superior alternative to traditionally used antibodies and could be utilized as artificial antibodies for the differentiation between viral and bacterial infections.

2. Materials and methods

2.1. Chemicals and Materials

Potassium hexacyanoferrate(III) ($K_3[Fe(CN)_6]$), potassium hexacyanoferrate(II) trihydrate ($K_4[Fe(CN)_6] \cdot 3H_2O$), Tween 20, Trisma base, glycine, and polyethylene glycol (PEG) were purchased from Sigma-Aldrich. Sodium perchlorate ($NaClO_4$, Fluka), PBS tablets (phosphate-buffered saline; 137 mM NaCl, 2.7 mM KCl, and 10 mM phosphate buffer, pH 7.4) in Biotechnology Grade, TM buffer (10 mM Tris-HCl + 10 mM $MgSO_4$), ethanol 96%, NaCl, HCl, $MgSO_4$, and $MgCl_2$ were purchased from Chempur (Poland). Wild-type bacteriophage (M13 KE phage (1.0×10^{10} plaque-forming units (pfu) pfu mL^{-1}), phages with a linear 12-mer peptide exposed on the protein III of M13KE phage (Ph.D-12 Phage Display Peptide Library), and *Escherichia coli* ER2738 were purchased from New England Biolabs, NEB. BactoAgar and LB were obtained from Roth (Germany).

Proteins: Human C-reactive protein (CRP) was bought from Biorbyt (UK). Myoglobin (Mb) from horse heart (90 %), troponin T (TnT) from human cardiac muscle (in the form of lyophilized powder), human serum albumin (HAS), interleukin-6 (IL-6), human serum normal, and bovine serum albumin (BSA) (lyophilized powder) were purchased from Sigma (USA). Fibrinogen (Fb) from human plasma was delivered by Lee Biosolutions (USA).

Carbon nanofibers (CNF) - were synthesized and characterized as reported in the literature [47]. Invitrogen™ Dynabeads™ M-270 Epoxy surface-modified magnetic nanoparticles (mNP) were purchased from Thermo Fischer Scientific (USA). Glassy carbon electrodes (GCE) (d = 2 mm) were purchased from Mineral Company. All chemicals were used without further purification. The sequencing of pIII gene of phage was performed by Genomed (Poland).

2.2. CRP binding bacteriophage isolation and characterization

In order to select bacteriophages that bind to CRP, a panning procedure was performed in the way described in the Phage Display Manual (NEB) [48] and our previous studies [18]. First, a CRP solution (100 μg mL^{-1}) was attached to the surface of magnetic nanoparticles beads (5 mg) (modified with epoxy groups, which enable the formation of amide bonds with CRP) to perform the screening process three-dimensionally and also to utilize a magnetic field to separate bound and unbound phages. The conjugation/incubation of the CRP to Dynabeads™ M-270 was performed with the addition of buffers, 3 M ammonium sulfate in 0.1 M sodium phosphate buffer pH 7.4, and 0.1 M sodium phosphate buffer pH 7.4, as recommended. After overnight incubation, coated beads were washed four times using 0.1% PBST (PBS , 0.1 % Tween-20). Then, 0.1% BSA in PBS solution was added to the obtained conjugate (CRP-mNP) in order to eliminate/block unspecific binding sites. Next, 10 μL of Phage Display Peptide Library was added to the CRP-mNP solution and incubated for one hour at room temperature (RT) with gentle shaking. The time of incubation has been optimized and is explained in more detail in our previous study [18]. Unbound phages were separated from CRP-mNP using a magnetic rack. The CRP-mNP were washed: six times using 0.1% PBST (in the first panning) and ten times with 0.5% PBST (in the next two pannings). Phages that bound CRP were eluted with 1 mL of 0.1 M glycine in HCl buffer (pH 2.2) for 10 min. The eluted phage solution (E1) was collected (using a magnetic rack) and directly titrated and amplified. Amplification of the phage has been performed in *Escherichia coli* ER2738 (NEB) according to the NEB protocol [48]. This procedure was used again in the next panning. After amplification, phages were used for the subsequent panning. A total of three rounds of panning were performed following the procedure described above. Following the last panning step, the eluted phages E3 were titrated on double-agar plates containing IPTG/X-gal. In the end, whole plate titration was performed from the E3 lysate to obtain single phage clones. Ten phage-clones were selected and amplified using the same procedure as reported above. The DNA strands were isolated from the selected ten phages, purified in the way described by Wilson [49] and sequenced commercially using the 96 *gpIII* sequencing primer (NEB).

In order to characterize the selected clones, the value of the binding efficiency for CRP binding was calculated for each of them. The binding efficiency is presented as O/I – a ratio of the output phage number (phages eluted/O) to the input phage number (phages incubated/I with the target protein, CRP). The P2-CRP phage were selected for further studies based on a high binding efficiency (1.32×10^{-4} for n=3 (RSD 5.6×10^{-5})) and on a high concentration after amplification. As a control, wild-type M13 phage was used. The panning procedure was performed for the control phage in the same way as described above. The same volume (10 µL) and the same concentration (1.0×10^{10} pfu mL^{-1}) of the wild-type M13 lysate was added to a new suspension of CRP-mNP. The value of the binding efficiency, which was 1.6×10^{-6}, was calculated in the same way.

The selectivity of the selected P2-CRP phage against other proteins was investigated. For this purpose, the panning was performed for these selected proteins (human serum albumin, interleukin-6, myoglobin, troponin T, and fibrinogen) with the CRP-binding phage (P2-CRP). The same volume (10 µL) and the same concentration (1.6×10^{12} pfu mL^{-1}) of the P2-CRP lysate was added to a new suspension of either HAS, IL-6, Mb, TnT, Fb-mNP, with the same concentrations, separately. Eluted phages from the corresponding protein suspension were titrated, and the binding efficiency assay parameters were calculated analogously as it was done for CRP.

2.3. Surface characterization

TEM analysis

Suspensions of CNF (3 mg mL^{-1}), P2-CRP phages (1.6×10^{11} pfu mL^{-1}) and P2-CRP phages with CNF (3 mg mL^{-1}) were adsorbed onto carbon-coated copper grids (Sigma) for 3 minutes and stained with 1.5% uranyl acetate. The samples were imaged and the images processed with iTEM software.

X-ray photoelectron spectroscopy (XPS)

Samples were prepared as follows: 10 µL droplets of the P2-CRP phage (1.6×10^{10} pfu mL^{-1}) suspension, 10 µL CNF suspensions (3 mg mL^{-1}), or the same volume of the CNF suspensions with P2-CRP were deposited on silicon wafer surfaces. Next, they were left to dry at room temperature. All further technical details were consistent with those in our earlier studies [18].

2.4. Electrode modification

A surface of a glassy carbon electrode (GCE) was first polished with alumina powder (diameter = 0.05 µm), then rinsed with water followed by 20 minutes of sonication first in water and next in ethanol. Then alternately 2 µL of the solution of negatively charged bacteriophage (M13 or P2-CRP, 1.0×10^{6} or 1.6×10^{6} pfu mL^{-1}) and 2 µL of the positively charged CNF suspension (3 mg/mL of CNF aqueous suspension) were deposited onto the GCE. This process was repeated to give one, three,

or five layers on the GCE labelled as 1,3,5L-M13(P2-CRP)/CNF. In the present study, "one layer" denotes a combination of a layer of the phage and CNF. GCE electrodes modified with only CNF or only M13/(P2-CRP) deposits were labelled as CNF and M13/(P2-CRP). The illustration for electrode modification with M13 or P2-CRP and CNF is presented in Schematic 1.

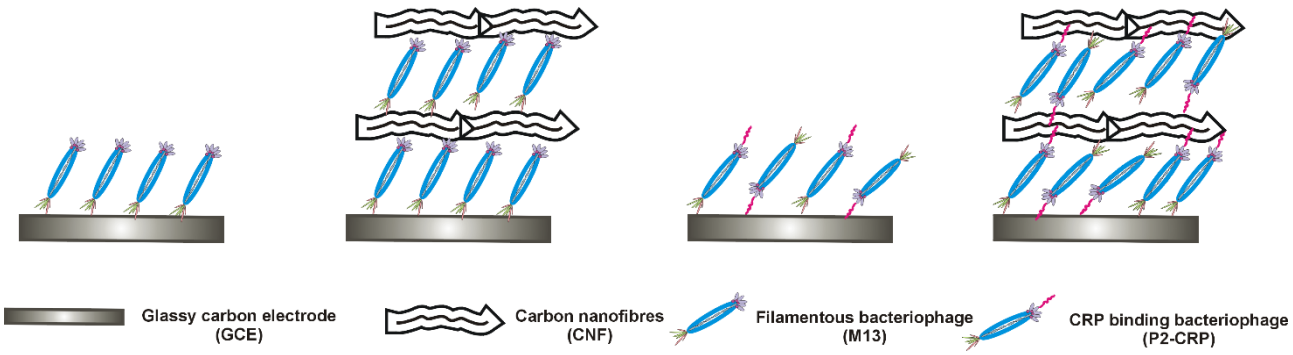

Schematic 1. An illustration of the GCE modification with an M13 wild bacteriophage, CRP binding bacteriophage (P2-CRP), CRP binding bacteriophage, and carbon nanofibers M13(P2-CRP)/CNF) employing the layer-by-layer method.

2.5. Apparatus

A three-electrode cell was used for performing electrochemical experiments, with a glassy carbon electrode (GCE) or modified GCE, a platinum wire (d = 0.5 mm), and an Ag|AgCl|KCl_{sat} electrode employed as the working, counter, and reference electrodes, respectively. Cyclic voltammetry measurements were performed using a μAutolabIII (Metrohm Autolab) potentiostat powered by GPES 4.9 software. All experiments were performed at ambient temperature (22 ± 3 °C). XPS analysis was performed with a Scanning XPS Microprobe instrument - PHI 5000 VersaProbe (ULVAC-PHI, Japan/USA); details are described elsewhere [18]. TEM images were obtained and analyzed with a transmission electron microscope (Tecnai G2 Spirit BioTWIN). Demineralized and ultrapure water, with a specific resistivity of 18.2 MΩ cm, from a water purification system (Sartorius), was utilized for experiments.

3. Results and discussion

The phage-display method was employed to identify bacteriophage, which selectively binds to CRP. The technique was based on several subsequent biopanning steps. Selection is made from a population containing a large number of variants of phages (a combinatorial phage library) using an approach resembling natural selection (directed evolution). We have used a commercial Phage Display Peptide Library (NEB) containing phages with peptides of 12 amino acids exposed. After

three cycles of biopanning, ten clones have been selected and verified based on the analysis of the value of the binding efficiency (O/I). The clone named P2-CRP exhibited the highest O/I of the tested phages (1.32×10^{-4} for n = 3 (RSD 5.6×10^{-5})). The obtained O/I values are two to four orders of magnitude higher than those obtained for other clones (3.57×10^{-6} – 7.50×10^{-8}), e.g., P1 (3.57×10^{-6}), P4 (4.0×10^{-7}) and P8 (5.0×10^{-8}) (Fig. 1). Also, the binding efficiency of this selected phage towards CRP is two orders of magnitude higher in comparison to the wild type phage (Fig. 1). The sequence analysis of the pIII gene of the P2-CRP phage revealed that the 12-mer peptide is expressed at the N-terminus of the protein pIII. The amino acid sequence is presented as follows: GGSDPEGMQGNY (pI = 3.29).

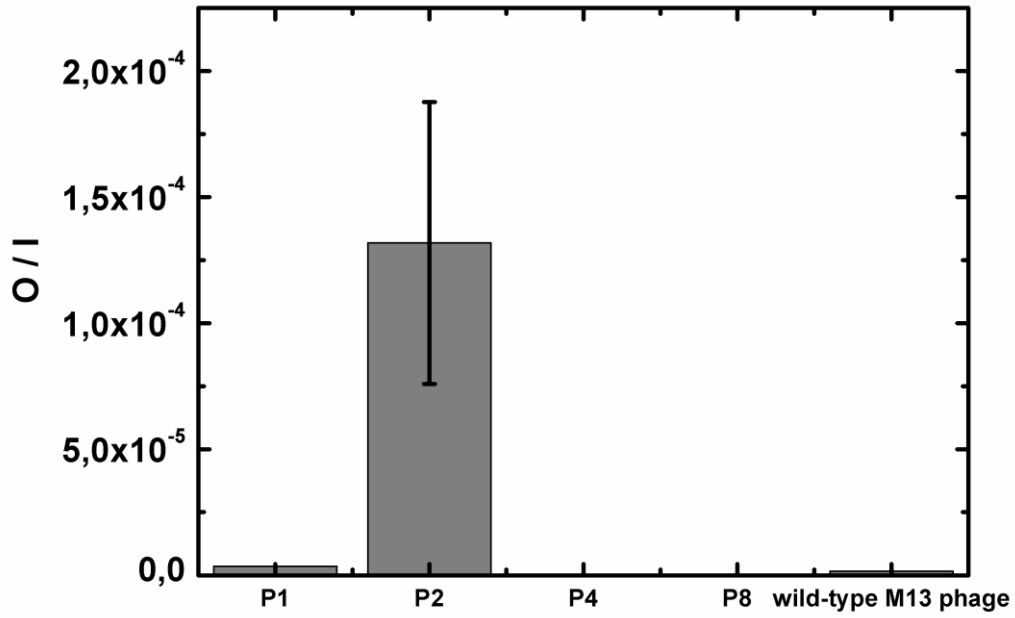

Fig. 1. The efficiency of CRP binding by the selected clones of phages: P1, P2, P4, P8 -CRP phage, and by the wild type phage M13.

Next, the binding efficiency assay of the P2-CRP phage was performed for myoglobin, fibrinogen, human serum albumin, interleukin-6, and troponin T. These proteins have been selected because of their presence in the human blood (HSA), participation in inflammatory reactions (IL-6), similar size to CRP (Fb), or/and usefulness in examination with other disease markers, like cardiovascular markers (Mb, TnT). The highest binding efficiency (O/I) was obtained for CRP, which is 1.88×10^{-4}, then for Fb 5.00×10^{-6}, TnT 1.75×10^{-6}, IL-6 1.05×10^{-6}, and the lowest for Mb and HSA, 2.5 ×

10^{-7} and 2.25×10^{-8}, respectively. The obtained values of the O/I for control/interfering proteins are comparable with the value obtained for wild-type phage with CRP and about two to three orders of magnitude lower than that obtained for the P2-CRP phage and CRP (Fig. 1). The obtained O/I values indicate that the P2-CRP phage binds most strongly with the CRP. Thus, P2-CRP has been used as a recognition element for creating new sensing platforms in our further studies. Phages selected via phage display technology have already been used for recognition of various disease markers [24,25,50]. However, currently, there are no reports on CRP-binding phages used as a sensor recognition element.

In order to prepare a biosensing platform based on the new CRP-binding phage, the layer-by-layer method was applied for immobilization of the phage together with carbon nanofibers (CNFs). The presence of the CNFs improves the electrical conductivity of the material, and it increases the surface area and the number of binding sites for CRP. The electrostatic interactions between the negatively charged phages (wild or CRP-binding) and positively charged carbon nanofibers enabled film formation on the electrode surface. These interactions have been utilized previously for the preparation of wild-type M13/CNF based electrode [17]. However, in this case, the LbL approach is utilized for electrode modification, while in the previous studies drop-casting was applied [17]. Electrostatic wild-type M13 phage interactions and aggregation into membranes were recently reported [51].

First, the selected CRP-binding bacteriophage, on its own, and with CNF conjugated, were investigated and characterized by transmission electron microscopy (TEM). Images in Fig. 2A, 3A show fibers of the P2-CRP phage with a length of ca. 1 μm, which is similar to the length of wild type M13 (Fig. 2B) and consistent with the literature data [52]. Also, some aggregates of the P2-CRP phage fibers are visible. The aggregation effect is well-known in the literature. Filamentous bacteriophage fibers tend to interact with each other forming self-assembled/organized aggregates and structures [18,53]. However, the aggregates of the P2-CRP fibers differ from the aggregates of the wild-type M13. From TEM images can be seen that the P2-CRP fibers (Fig. 2A) have a greater tendency to self-assemble compared to the more separated M13 fibers (Fig. 2B). The effect might result from the presence of the 12-mer peptide exposed on the surface of the P2-CRP. The sequence of the modified peptide has among neutral amino acids also aspartic and glutamic acids, which are negatively charged, thus increasing the total negative surface charge of the P2-CRP phage. This extra negative charge can induce changes in overall charge and thereby additional interactions between P2-

CRP fibers. Furthermore, tyrosine and methionine are present, which might lead to additional π–π stacking and van der Waals interactions between P2-CRP fibers.

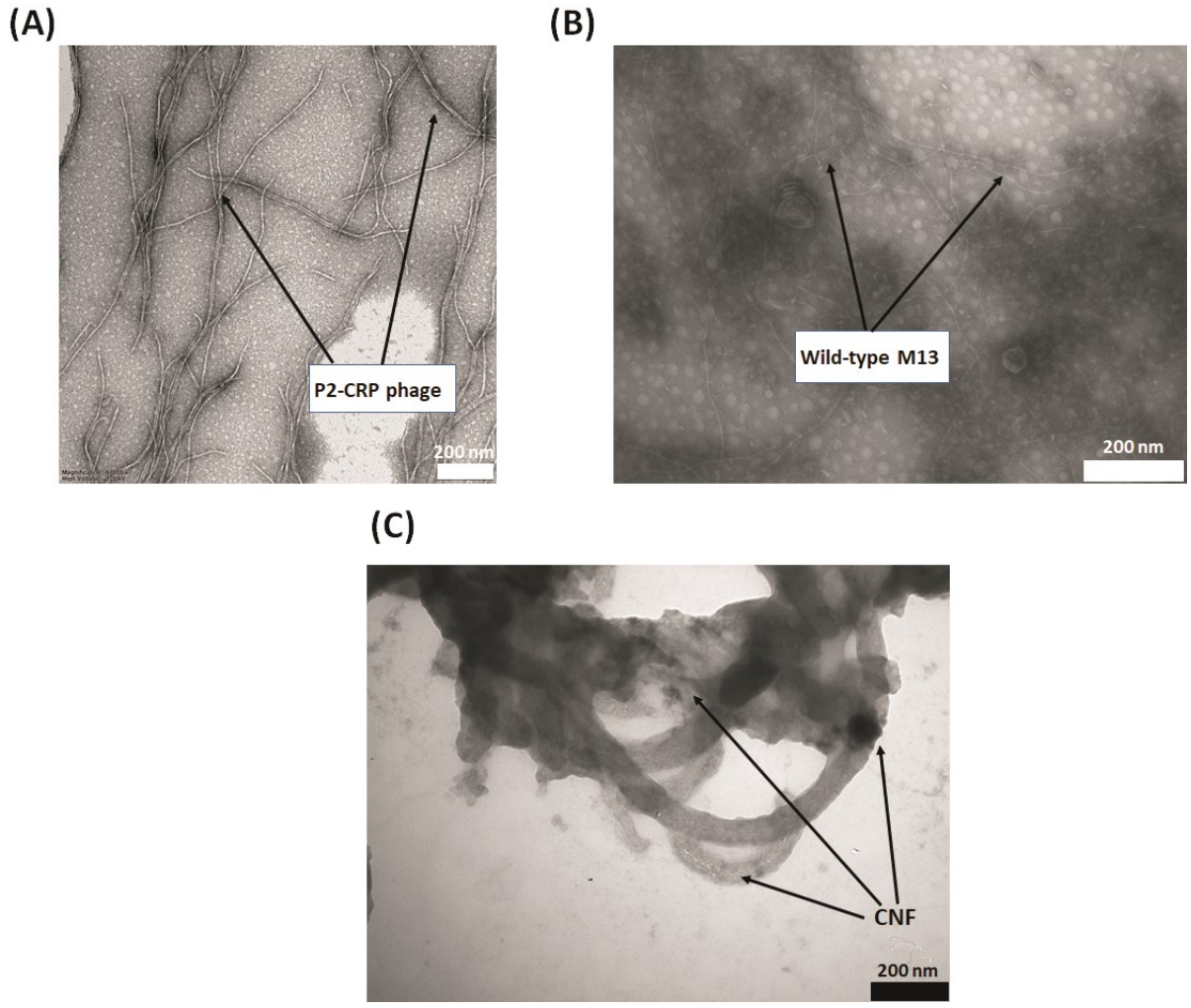

Fig. 2. TEM images of (A) P2-CRP phage (B) wild-type M13 and (C) carbon nanofibers (CNF). Scale bar: 200 nm.

The CNFs alone form unordered, tangled structures (Fig. 2C), which differ from the structures in the presence of the P2-CRP phage. Images in Fig. 3B show interactions of P2-CRP phage with CNFs. P2-CRP fibers in the presence of the CNFs line up, intersecting each other, and form a unique carpet-like structure (Fig. 3B (i, ii)). Based on TEM images, it can be seen that P2-CRP phages are specifically attached to CNF via their endings and their edges. P2-CRP and CNF fibers aggregate into organized 3D layered structures of the size of a few hundred nanometres (Fig. 3B (ii)). Such an alignment of M13 phage with CNFs has not been observed. M13 phages bind to CNFs non-specifically via different proteins, thereby forming disordered structures [17]. A phage selected by

phage-display has been reported to bind specifically CNF only via endings [18]. As can be seen, the presence of the peptide on the P2-CRP surface affects not only interactions between the P2-CRP phage fibers but also between those fibers and CNF.

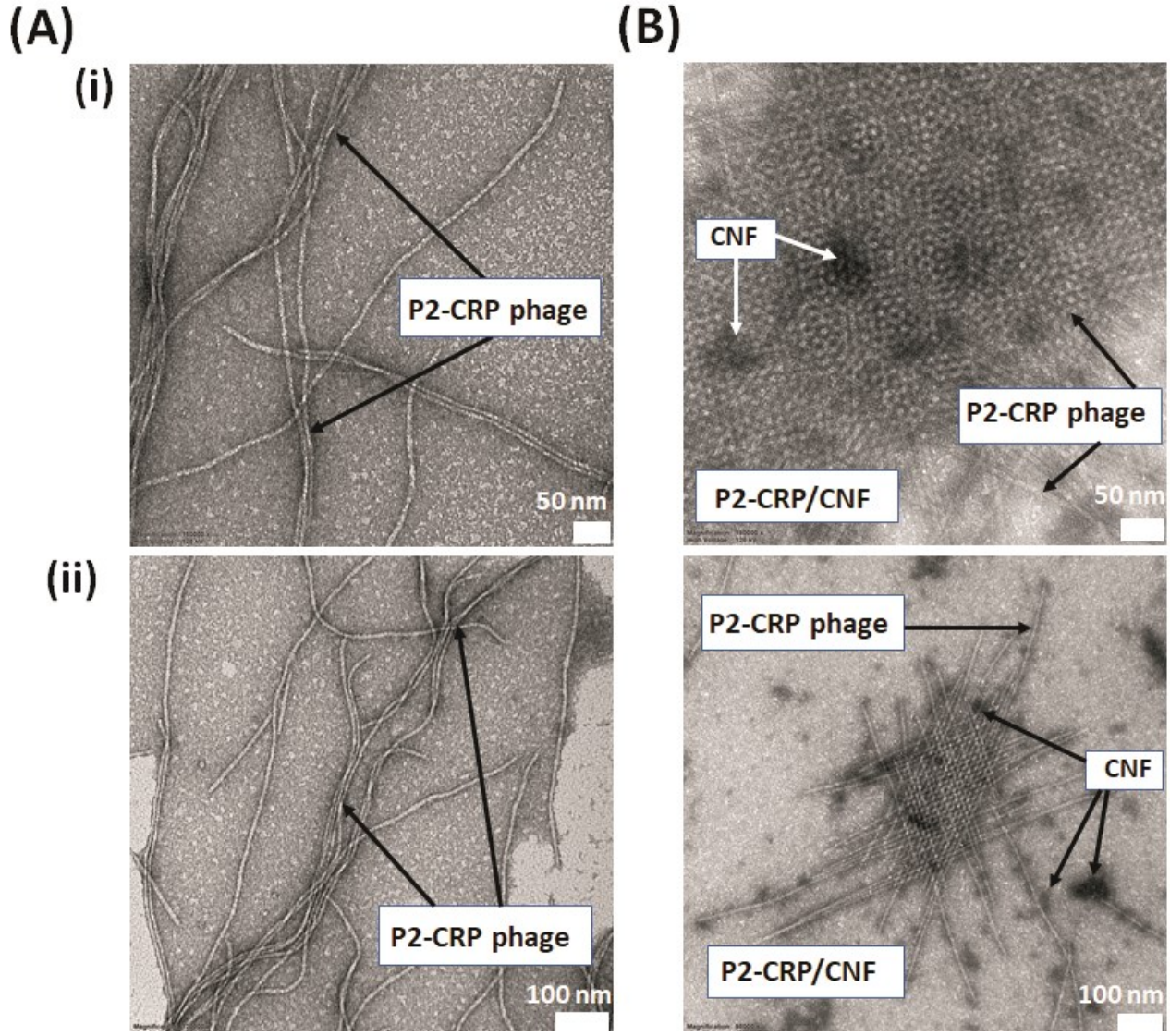

Fig. 3 TEM images of selected phage (A) P2-CRP and (B) P2-CRP phage with CNF (P2-CRP/CNF). Scale bar: (i) 50 nm and (ii) 100 nm.

XPS surface analysis was performed to gather more information about the new material P2-CRP/CNF. The XPS spectra were collected for all samples: CNF, P2-CRP phage, and conjugate P2-CRP/CNF. In the case of CNF alone, only two peaks from carbon C1s and oxygen O1s were recorded (Table 1, see Supplementary Fig. F1). The obtained results are in agreement with the literature [54]. The spectra gathered for P2-CRP/CNF material do not reveal any additional peaks in comparison to

P2-CRP only, indicating similar elemental surface composition (see Supplementary Fig. F2). A difference in the relative atomic percentage of aliphatic carbons between the P2-CRP/CNF (34.37 %) and P2-CRP (13.80 %) is observed (see Table 1). The results indicate that some amine groups of P2-CRP phage could interact with CNF carboxylic acid groups, probably via electrostatic interactions. The peak at 286.4 eV, which could be attributed to -C-OH, recorded for P2-CRP (see Supplementary Fig. F2 A (i)) is up-shifted in comparison to P2-CRP/CNF (see Supplementary Fig. F2 B (i)). In the case of the O1s XPS spectra, both analyzed samples (P2-CRP and P2-CRP/CNF) reveal two peaks for O=C–OH (carboxyl, 531.1, 531.2 eV) and for O (carbonyl, 533.0, 532.5 eV) groups, which differ significantly in their intensity (Fig. Supplementary Fig. F2 (ii), Table 1). An up-shifting and decrease in the carboxyl peak intensity for P2-CRP in comparison to P2-CRP/CNF are observed (Supplementary Fig. F2 A, B (ii)). The peak at around 535 eV can be attributed to some physisorbed water [55]. The XPS N1s spectra recorded for P2-CRP/CNF reveal significant dissimilarities in the content of the nitrogen and the number of N1s peaks compared to P2-CRP (Table 1). Beyond the peaks at 399.7 400, 400.9 eV, which are attributed to $-NH_2$ and amine plane –NH- groups, an additional peak at 402.2 eV assigned to protonated amino groups ($-NH_3^+$) are observed for P2-CRP/CNF (Table 1). This peak has not been present in the XPS spectra recorded for wild-type M13 with CNF [17]. The content of the nitrogen for P2-CRP/CNF is almost four times higher than for P2-CRP (Table 1). This result may indicate that more amide bonds have been formed between the P2-CRP phage and CNF through high phage loading on the CNF surface. The result also confirms that mainly non-covalent binding via electrostatic interactions is responsible for binding the P2-CRP to CNFs. The same was also observed previously for the CNF based materials with wild-type M13 or with phage selected via phage display technology [17,18].

Table 1 XPS analysis of P2-CRP bacteriophage, P2-CRP/CNF, and CNF suspension (surface composition expressed as an atomic percentage).

chemical state	concentration / at.%		
	P2-CRP	**P2-CRP/CNF**	**CNF**
C1s – 284.6, 284.8 eV (C-C_{arom}, CH)	13.80	34.67	66.60
C1s – 285.6 eV (C-C, CH2 groups)	-	-	8.70
C1s – 286.0, 286.4 eV (C-OH, C-NH_2)	44.10	21.73	-
C1s – 286.5 eV (C-OH)	-	-	4.70
C1s – 287.8, 287.5, 288.1 eV (C=O) ketone	5.1	10.97	2.6
C1s – 288.8, 288.9 eV (O=C−N; O=C−C) carboxylate	-	-	4.30
C1 – 290.9 eV ()	-	-	4.30
C1s – 292.3, 292.7 eV (carbonate)	-	1.81	1.50
C1s total	**63.00**	**69.18**	**92.70**
O1s – 531.1, 531.2 eV (C-OH)	3.1	9.72	0.6
O1s –532.5, 533.0 eV (C=O)	29.4	6.83	6.6
O1s – 534.3, 535.9 eV (H_2O, CO ads)	2.0	3.32	-
O1s total	**34.50**	**19.87**	**7.30**
N1s – 398.2 eV (pyridinic nitrogen)	-	0.76	
N1s –399.7 400 eV (C-N, C-NH_2, C-O)	2.5	8.82	
N1s – 400.9 eV (N-H, -NH_3^+)	-	0.97	
N1s – 402.2 eV (NH3+)	-	0.39	
N1s total	**2.5**	**10.94**	-

Cyclic voltammetry was utilized to characterize the electrochemical behaviour of the new P2-CRP/CNF material. First, electrodes modified with P2-CRP and wild-type M13 phages were analyzed. For this purpose, lysates of phages (with the same concentrations), wild-type M13 phage (1.0×10^6 pfu mL^{-1}), and selected P2-CRP phage (1.6×10^6 pfu mL^{-1}) were separately deposited on GCE electrode surfaces. The selected concentration of the phage lysate (1.6×10^6 pfu mL^{-1}) was chosen based on experiments with different phage concentrations (1.6×10^8, 1.6×10^{10}, 1.6×10^{14} pfu mL^{-1}). It was observed that the phage concentration does not significantly affect the electrochemical response of the phage-modified electrode (data not shown). The experiments with GCE modified with P2-CRP or M13 were performed with an outer-sphere electron transfer redox probe, $Fe(CN)_6^{3-/4-}$. As one can see from the cyclic voltammograms, the values of the peak current for the M13 (Fig. 4b) and P2-CRP (Fig. 4c) electrodes are smaller than those observed with the bare GCE (Fig. 4a). The smaller currents indicate partial blocking of the electrode surface by the hydrophobic phage layer and/or weak wetting with the aqueous electrolyte. The peak-to-peak separation for the GCE modified with phages (M13 or P2-CRP) is larger than that for the bare GCE The considerable broadening in the current peak widths for the P2-CRP phage (Fig. 4c) reflects a slow electron transfer reaction could be linked to P2-CRP being more hydrophobic compared to M13. A combination of higher hydrophobicity and a stronger electrostatic repulsion between the negatively

charged P2-CRP and $Fe(CN)_6^{3-}$ anions are likely to cause the change in shape observed in voltammograms. The pI of the M13 equals 4.2, so in PBS, it is negatively charged. On the surface of the P2-CRP phage, the 12-mer peptide is exposed with a pI of 3.9 (the pI was calculated using commercial software http://isoelectric.org/). Due to the presence of aspartic and glutamic acids, which are negatively charged amino acids, the total surface charge of the phage is extra negative when compared to M13. This extra charge can cause stronger repulsion between P2-CRP and $Fe(CN)_6^{3-}$. The sequence of the exposed peptide also contains tyrosine and methionine, which might be responsible for additional interactions via π–π stacking and via van der Waals interactions to CNFs. We assume that these specific interactions result in different electrochemical behaviour of the electrode modified with the P2-CRP compared to the electrode modified with M13 phage. This result is consistent with TEM analysis (see Fig. 2).

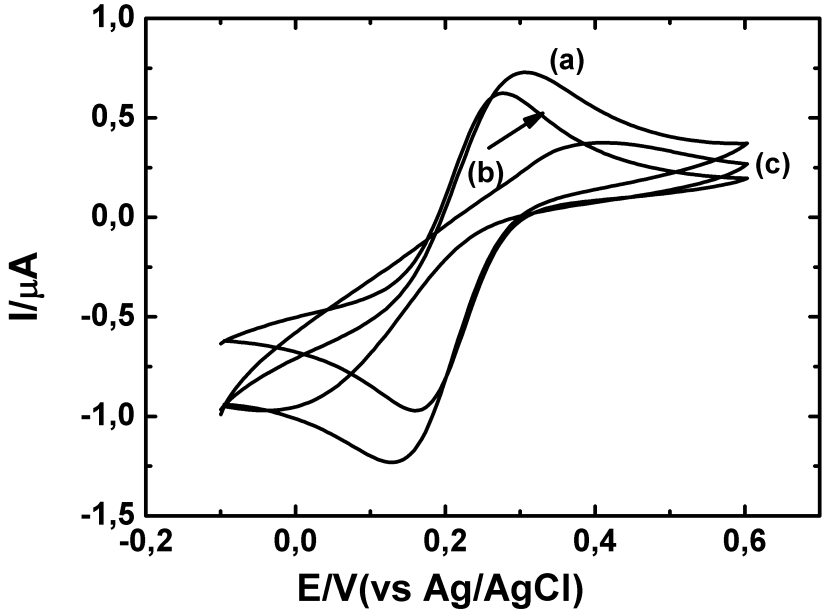

Fig. 4 Cyclic voltammograms (2nd potential cycle) of (a) a bare GCE electrode or coated with (b) wild-type M13 bacteriophage (c) and P2-CRP-binding bacteriophage immersed in 1 mM $K_3[Fe(CN)_6]$ solution in PBS (137 mM NaCl, 2.7 mM KCl, and 10 mM phosphate buffer, pH 7.4). Scan rate 10 mV s^{-1}.

Next, in order to simultaneously improve the electrical conductivity of the phage modified electrode and to increase the number of phages on the electrode surface, CNFs were introduced. A modified electrode was obtained by the LbL method. The phages are negatively charged, carboxylic groups

from Glu2, Asp4, Asp5, Asp12, and Glu20 are located on the major capsid [56], and additional Asp, Glu on the exposed peptide in the case of P2-CRP. To achieve a well-defined surface modification, the electrostatic interactions between the phages and positively charged CNFs in suspension (confirmed by values of zeta potential dissolved in water ($\zeta = + 21.3 \pm 1.31$ mV [17]) were utilized. This type of surface modification for phage immobilization on the electrode surface has not been previously reported. An electrostatic multilayer film, which comprises negatively charged polyanions (poly(acrylic acid)) and positively charged polycation (poly(ethyleneimine)), was reported as a platform for M13 phage adsorption [57,58]. The LbL approach has been used previously for the immobilization of genetically modified M13 phage by Belcher and coworkers with a covalent binding strategy for phage attachment [46].

The GCE electrodes modified with 1 and 3 layers (denoted 1L-M13(P2-CRP)/CNF and 3L-M13(P2-CRP)/CNF) were examined in the presence of the redox probe $Fe(CN)_6^{3-}$. As shown in Fig. 5, the values for the capacitive current and the faradaic current recorded for M13/CNF (Fig. 5A) and P2-CRP/CNF (Fig. 5B) electrodes increased with the number of layers/materials deposited on the electrode surface. In the case of the M13/CNF electrode, the highest value of the current was obtained for electrodes modified with three layers (Fig. 5A(c)) in comparison with data for 1L-M13/CNF (Fig. 5A(b)), bare GCE (Fig. 5A(a)), and CNF modified GCE (Fig. 5B(d)). This result is linked to the electroactive surface area. The same trend was observed for the P2-CRP/CNF electrodes (Fig. 5B). However, a higher value of the peak current was recorded for 1,3L-P2-CRP/CNF (Fig. 5B (c) compared to that for 1,3L-M13/CNF (Fig. 5A (c)). These results arise probably from the fact that P2-CRP phage with extra 12-mer peptide interacts with CNF differently compared to the interaction with M13 (Fig. 3), allowing for more CNF attachment to the electrode surface. Thus, these electrodes give well-assembled conductive material, which provides a higher peak current compared to the case of M13/CNF. Additionally, it can be seen that the cathodic peak potential of the 3L-P2-CRP/CNF modified electrode (Fig. 5B(c)) is shifted by 64 mV towards negative potentials in comparison to that for the 3L-M13/CNF modified electrode (Fig. 5A(c)) and the peak-to-peak separation is increased. Both could be linked to higher background currents causing some Ohmic distortion. No further increase of the faradaic current is observed when the electrode is modified with 5L-M13/CNF, because the electrochemical reaction occurs only at the outer layer of M13/CNF. The electrode modified with 3L of CNF is mechanically unstable (data not shown).

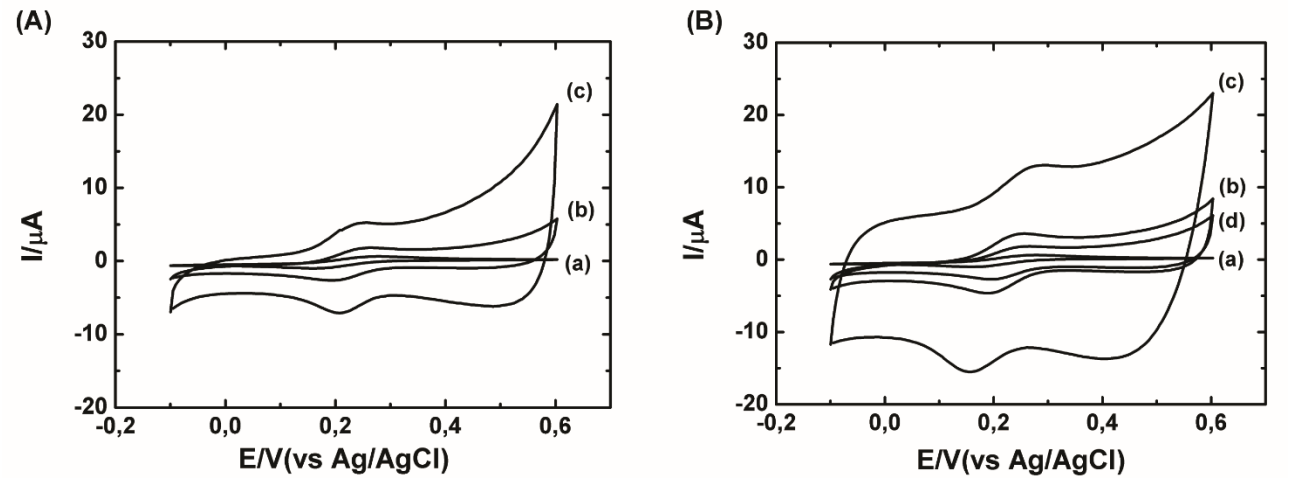

Fig. 5. (A) Cyclic voltammograms (2nd potential cycle) of (a) a bare GCE electrode or coated with (b) one (c) three layers of M13/CNF immersed in 1 mM $K_3[Fe(CN)_6]$ solution in PBS. Scan rate 10 mV s^{-1}. (B) Cyclic voltammograms (2nd scan) of (a) a bare GCE electrode or coated with (b) one (c) three layers of P2-CRP/CNF (d) carbon nanofibers immersed in 1 mM $K_3[Fe(CN)_6]$ solution in PBS. Scan rate 10 mV s^{-1}. PBS (137 mM NaCl, 2.7 mM KCl, and 10 mM phosphate buffer, pH 7.4).

In subsequent studies, the ability of the selected P2-CRP phage to detect CRP is investigated. Firstly, 2 μL of the P2-CRP phage lysate (1.6×10^6 pfu mL^{-1}) was deposited onto the electrode surface by drop-casting. After drying, the obtained electrode was examined in a solution containing 2.5 mM $[Fe(CN)_6]^{3-}$ and 2.5 mM $[Fe(CN)_6]^{4-}$ in the presence of CRP at different concentrations from 4 to 40 μg mL^{-1}. After the addition of the CRP to the solution, the anodic peak currents are decreasing (see Fig. 6A), with a linear dependence on CRP concentration (Fig. 6A inset). The decrease in peak current indicates that the P2-CRP binds the CRP. Owing to bound CRP blocking the electrode surface, electron transfer is hindered. Next, the control experiment was performed with an electrode modified with M13 phage (1.0×10^6 pfu mL^{-1}). Measurements were performed in the presence of CRP in the same range of concentrations (4 to 40 μg mL^{-1}). Fig. 6B (b-d) show that the addition of CRP with concentrations from 4 to 20 μg mL^{-1} causes values of the anodic currents to only change slightly. This result shows that M13 does not specifically recognize the CRP protein. A decrease in the current is observed only at the highest concentration of CRP (40 μg mL^{-1}) (Fig. 6B (e) inset). This is likely to result from non-specific interactions. As the CRP is established as one of the cardiac markers, the selectivity of the P2-CRP phage was studied in comparison to related markers. For this purpose, the electrode modified with P2-CRP phage was prepared and examined in the presence of another cardiac marker - myoglobin (Mb) - at concentrations from 4 to 40 μg mL^{-1}. From the cyclic voltammetry

data, it can be seen that the peak current after the addition of the first portion of Mb (4 μg mL^{-1}) is even slightly increasing (Fig. 6C (b)) in comparison with bare GCE (Fig. 6C (GCE)). This current increase might indicate that the Mb due to its smaller size (17.8 kDa) in comparison to pentameric CRP (120 kDa) can more easily penetrate the hydrophobic layer of the P2-CRP. The interactions could make the P2-CRP layer more hydrophilic, thereby improving electron transfer. After the addition of further portions of Mb (20 μg mL^{-1}), the anodic peak current is almost unchanged (Fig. 6C (c,d)). The decrease of the current is clearly visible only at the highest concentration of Mb (40 μg mL^{-1}) (Fig. 6C (e), inset). This outcome results from non-specific interactions between proteins (P2-CRP phage and Mb), similarly to the case observed for the electrochemical behaviour of the GCE-M13 in the presence of CRP. From these experiments and data analysis, it can be concluded that the P2-CRP phage-modified electrodes recognized the CRP in a selective and specific manner. The latter observation/conclusion can be supported by the fact that the electrostatic interactions between studied proteins (Mb and CRP) and the phage layer are unlikely because Mb (pI=6.8-7.4 [59]) and CRP (pI =5.3 and 7.4) are electrically neutral in solutions at pH 7.4. For binding of CRP by P2-CRP probably mainly specific interactions are responsible, which result from the exposed 12-mer peptide.

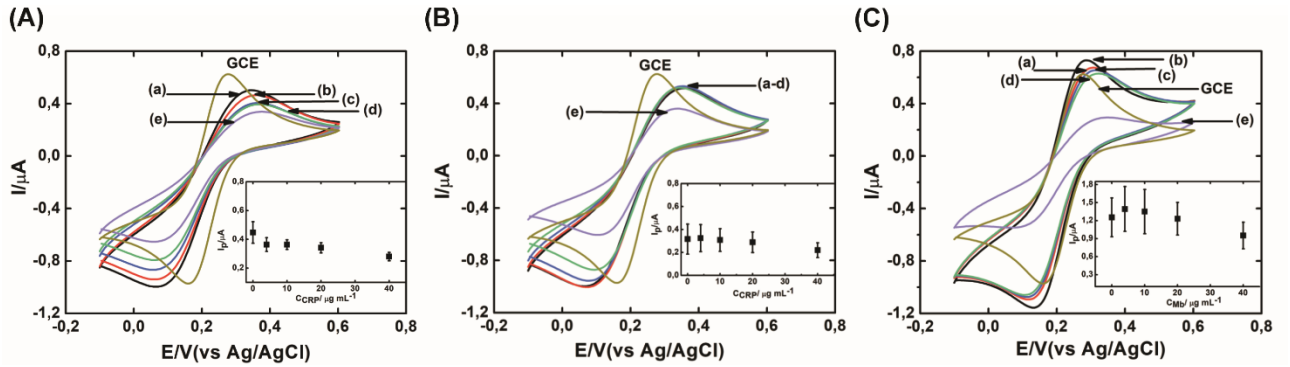

Fig. 6. (A) Cyclic voltammograms (2nd scan) of GCE electrode and coated with P2-CRP phage immersed in 2.5 mM $[Fe(CN)_6]^{3-}$ and 2.5 mM $[Fe(CN)_6]^{4-}$ in 0.1 M KCl aq containing (a) 0 (b) 4.0 (c) 10.0 (d) 20.0 and (e) 40.0 μg mL^{-1} of CRP. Scan rate 10 mV s^{-1}. Inset: The plot of peak current vs C_{CRP} concentration. (B) Cyclic voltammograms (2nd scan) of GCE electrode and coated with M13 phage immersed in 2.5 mM $[Fe(CN)_6]^{3-}$ and 2.5 mM $[Fe(CN)_6]^{4-}$ in 0.1 M KCl aq containing (a) 0 (b) 4.0 (c) 10.0 (d) 20.0 and (e) 40.0 μg mL^{-1} of CRP. Scan rate 10 mV s^{-1}. Inset: The plot of peak current vs C_{CRP} concentration. (C) Cyclic voltammograms (2nd scan) of GCE electrode coated with P2-CRP phage immersed in 2.5 mM $[Fe(CN)_6]^{3-}$ and 2.5 mM $[Fe(CN)_6]^{4-}$ in 0.1 M KCl aq containing (a) 0 (b) 4.0 (c) 10.0 (d) 20.0 and (e) 40.0 μg mL^{-1} of Mb. Scan rate 10 mV s^{-1}. Inset: The plot of peak current

vs C_{Mb} concentration. The presented results are average values from four experiments, with RSD represented by error bars.

In order to improve electrical conductivity and to increase the number of binding sites for CRP on the P2-CRP phage modified electrode, CNFs were introduced. As described above, the LbL approach was utilized, which enables the immobilization of the P2-CRP phage within the CNFs. The electrodes modified with 1 and 3L P2-CRP/CNF were prepared and used for CRP recognition. The current is decreasing for both of these electrodes (modified with one (see Supplementary Fig. F3) and three layers (Fig. 7)) when the CRP concentration increased from 4 to 40 μg mL^{-1}, which is consistent with observations for P2-CRP-modified electrodes (Fig. 6A). The highest value of the anodic peak current was recorded for 3L-P2-CRP/CNF (Fig. 7). The lowest value was obtained for P2-CRP modified electrodes (Fig. 6A). In the case of the 3L-P2-CRP/CNF electrode, after addition of the first part of CRP solution (0.04 μg mL^{-1}), the most visible drop in the peak current was recorded (Fig. 7). We hypothesize that at the 3L-P2-CRP/CNF electrode, the P2-CRP phage binds strongly to CNFs, thus forming effective percolation paths and that allow for appropriate electron transport. A high phage loading gives more binding sites for CRP. The latter effect was also confirmed by XPS analysis (see Table 1). Therefore, the electrode modified with 3L-P2-CRP/CNF was selected for further characterization in terms of CRP recognition. As depicted in the inset of Fig. 7, the peak current is decreasing with increasing concentration of CRP. The obtained calibration curve for CRP exhibits a wide linear range of 0.04 – 100 μg mL^{-1}. The regression equation is I = -0.1773c + 19.2967 (c is the CRP concentration) with a detection limit (LOD) (S/N = 3) of 0.04 μg mL^{-1}. The reproducibility of the 3L-P2-CRP/CNF electrode was calculated based on measurements performed for four electrodes for the same concentration of CRP (10 μg mL^{-1}) under the same conditions; the RSD was 9.85 %, n=3. The 3L-P2-CRP/CNF electrode maintains 80.71 % of its activity towards 10 μg mL^{-1} CRP recognition after 7 days of storage at 23 ºC; the RSD was 11.76 %, n=3. These results indicate good stability of the proposed CRP binding phage/CNF electrode. There is no requirement to keep sensor electrodes in a fridge like it is customary with most of the antibody-based sensing systems. Moreover, the sensing properties of the new CRP binding phage are comparable with other CRP recognition elements based electrode [31–33], making it possible to apply such phage as artificial antibodies in the future.

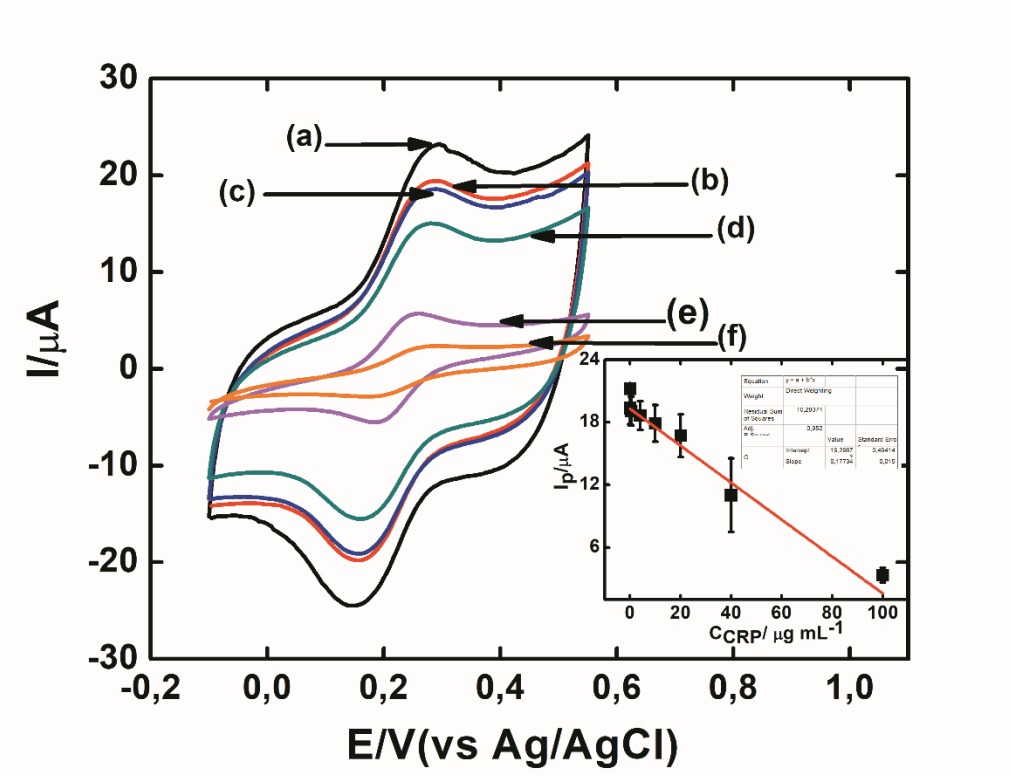

Fig. 7. Cyclic voltammograms (2nd scan) of GCE electrode coated with 3L-P2-CRP/CNF immersed in 2.5 mM $[Fe(CN)_6]^{3-}$ and 2.5 mM $[Fe(CN)_6]^{4-}$ in 0.1 M KCl aq containing (a) 0 (b) 4.0 (c) 10.0 (d) 20.0 (e) 40 and (f) 100 μg mL^{-1} of CRP. Scan rate 10 mV s^{-1}. Inset: plot of peak current vs C_{CRP} concentration. Results are average values from four experiments, with RSD represented by error bars.

The selectivity of the 3L-P2-CRP/CNF electrode has been tested in the same way as for the P2-CRP/M13 electrodes in the presence of Mb/CRP (see Supplementary Figure F4.). The 3L-P2-CRP/CNF electrode was examined in 2.5 mM $[Fe(CN)_6]^{3-}$ and 2.5 mM $[Fe(CN)_6]^{4-}$ solution in the presence of CRP at different concentrations from 4 to 40 μg mL^{-1}. After the addition of the CRP to the solution, the anodic peak currents are decreasing (see Supplementary Figure F4 ▲, Fig. 7). The drop of the current indicates that P2-CRP binds to CRP. Next, the control experiment was performed with an electrode modified with M13 phage (1.0×10^6 pfu mL^{-1}) (3L-M13/CNF). Measurements were performed in the presence of CRP at the same range of concentrations (4 to 40 μg mL^{-1}). As is presented in Supplementary Figure F4 (■), when the CRP at concentrations from 4 to 20 μg mL^{-1} is added to the solution, values of the anodic current are only slightly changing. The change is observed at the level of 20 % with respect to the initially added concentration of CRP. However, in the case of 3L-P2-CRP/CNF electrodes changes were higher with ca. 50 %. The smaller change shows that M13 does not specifically recognize the protein. A decrease of the current is observed only at the highest

concentration of CRP (40 μg mL^{-1}) (see Supplementary Figure F4 (■)). But this probably results from non-specific interactions between proteins. The 3L-P2-CRP/CNF electrode was prepared and examined in the presence of myoglobin (Mb) at the same concentration range (4 to 40 μg mL^{-1}). It can be seen that the peak currents after the addition of Mb are almost constant (Supplementary Figure F4 (●)). These results are consistent with data for P2-CRP/M13 electrodes (Fig. 6).

The selectivity of the GCE electrodes modified with P2-CRP phage and 3L-P2-CRP/CNF were tested in the presence of a proinflammatory cytokine – interleukin 6 under the same conditions. The results are presented in Fig. 8. When the electrodes were incubated with 2.5 µg mL^{-1} IL-6 solution (P2-CRP-IL-6 and 3L-P2-CRP/CNF-IL-6), the peak currents did not decrease. The responses of the electrode with/without the IL-6 were consistent. This result shows that the P2-CRP phage does not bind to selected proinflammatory proteins, only to CRP, and confirms a good selectivity of the electrode based on P2-CRP phage.

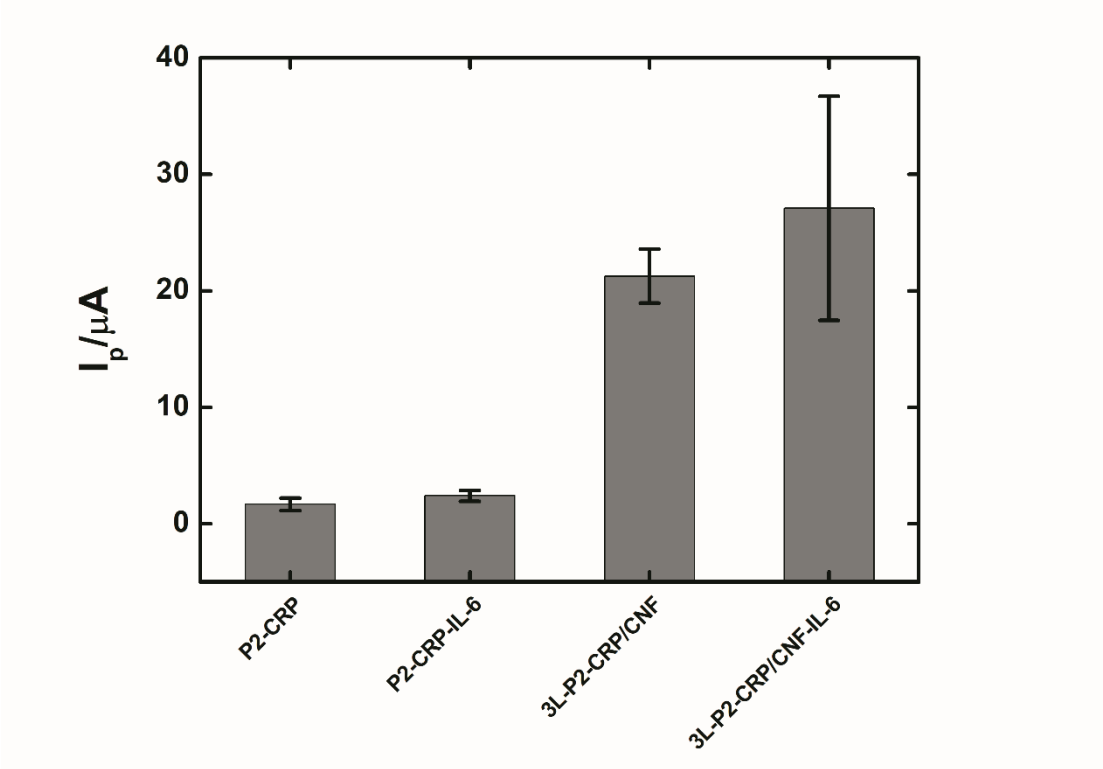

Fig. 8. The plot of peak current plotted against the response of the GCE electrodes modified with P2-CRP and 3L-P2-CRP/CNF in the absence and presence of the IL-6 (2.5 µg mL^{-1}) P2-CRP-IL-6, 3L-P2-CRP/CNF-IL-6. The results are average values from four experiments, with RSD represented by error bars.

To check the selectivity of the 3L-P2-CRP/CNF electrode additional experiments have been performed in a mixture of interferents/proteins (mixed proteins: TnT (2.5 μg mL^{-1}), Mb (2.5 μg mL^{-1}), HAS (2.5 μg mL^{-1}), Fb (2.5 μg mL^{-1}), BSA (2.5 μg mL^{-1})), natural human serum and at a specified concentration of CRP (4 μg mL^{-1}). The results are presented in Fig. 9. When the 3L-P2-CRP/CNF electrode was measured in the solution of the mixed protein or human serum, the current did not change significantly, and it remained comparable to that in blank experiments (Fig. 8). However, the addition of 4.0 μg mL^{-1} CRP solution into the mixed protein or human serum results in a decrease in peak current. In the case of the mixed proteins, the drop in the current is more visible. We hypothesize that one of the proteins decreases the hydrophobicity of the CNFs, making the 3L-P2-CRP/CNF more effective in the mixed protein solution. This does not occur in the case of the blank or the human serum. Nevertheless, these studies require further and more in-depth analysis. The outcomes of these preliminary experiments show that the 3L-P2-CRP/CNF electrode is sensitive in the presence of CRP and can be applied for recognition of this protein in different media.

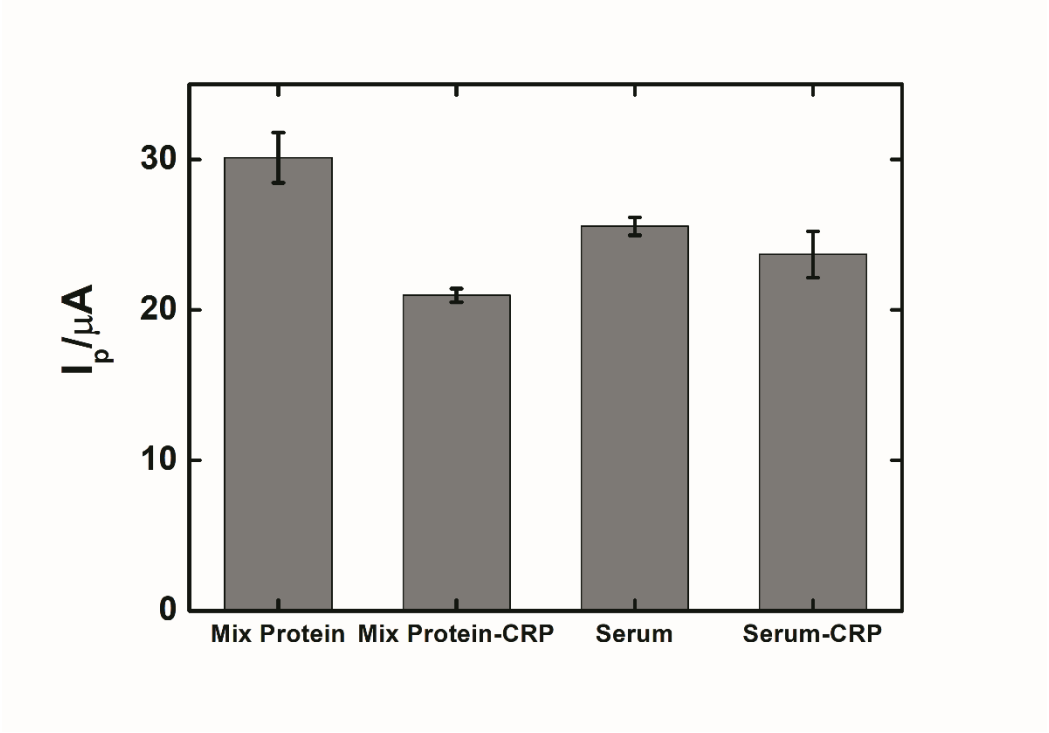

Fig. 9. The plot of peak current plotted against the response of the GCE electrodes modified with 3L-P2-CRP/CNF in the absence and presence of the CRP (4.0 μg mL^{-1}) in the mixed protein and in human serum. The mixed protein contains TnT (2.5 μg mL^{-1}), Mb (2.5 μg mL^{-1}), HAS (2.5 μg mL^{-1}), Fb (2.5 μg mL^{-1}), BSA (2.5 μg mL^{-1}). The results are average values from three experiments, with RSD represented by error bars.

The 1L- and 3L-P2-CRP/CNF electrodes operate in the same range (4-40 μg mL^{-1}) as the P2-CRP electrode, making them suitable for future application, for example, to differentiate between viral and bacterial infections. However, in the future, more analysis and studies will be required to perform and understand more thoroughly the interactions between the exposed peptide on the P2-CRP phage and the CRP.

4. Conclusions

In this study, the phage display technology has been utilized for the generation of a new sensing element for C-reactive protein (one of the markers of inflammatory processes in the human body) recognition. The high binding efficiency of this new element towards CRP has been studied and confirmed in contrast to wild-type M13 and other proteins using biological methods.

The selected phage, with a net negative surface charge, has been used in combination with positively charged carbon nanofibers for electrode modification via the LbL method. Electron microscopy shows that the CRP-binding phage binds to CNF via ends and edges, forming ordered carpet structures. XPS analysis reveals that the selected phage interacts with CNF mainly via electrostatic interactions / non-covalent bonding. These interactions have been utilized for the CRP-binding phage immobilization on the electrode surface in the presence of CNFs. The role of the phage is twofold, as building blocks and as sensing elements. The electrostatically LBL assembled phage-CNF electrode has been used successfully for CRP recognition. The sensor operating range enables applications, for example, in the differentiation between viral and bacterial infections. The stability, reproducibility, and selectivity of the electrode modified with CNFs and phage have been demonstrated using electrochemical measurements.

The new CRP-binding phage could become an alternative to traditionally used antibodies and can be utilized as artificial antibodies for the differentiation between viral and bacterial infections, thereby decreasing the antibacterial resistance problem. Additionally, phages in comparison to antibodies are more robust, cheaper, and their production is possible on a large scale.

AUTHOR INFORMATION

Corresponding Author

*E-mail: kszot@ichf.edu.pl. Tel: +48 223433130, fax: +48 223433333

Notes

The authors declare no competing financial interest.

Acknowledgements

This work was funded by the Polish National Science Centre via a SONATA 13 grant UMO-2017/26/D/ST5/00980 to Dr. Katarzyna Szot-Karpińska and also financial support from the project 3/DOT/2016 funded by the City of Gdynia, Poland is acknowledged. KSK would like to acknowledge Dr. Marcin Pisarek for XPS analysis.

Graphical Abstract

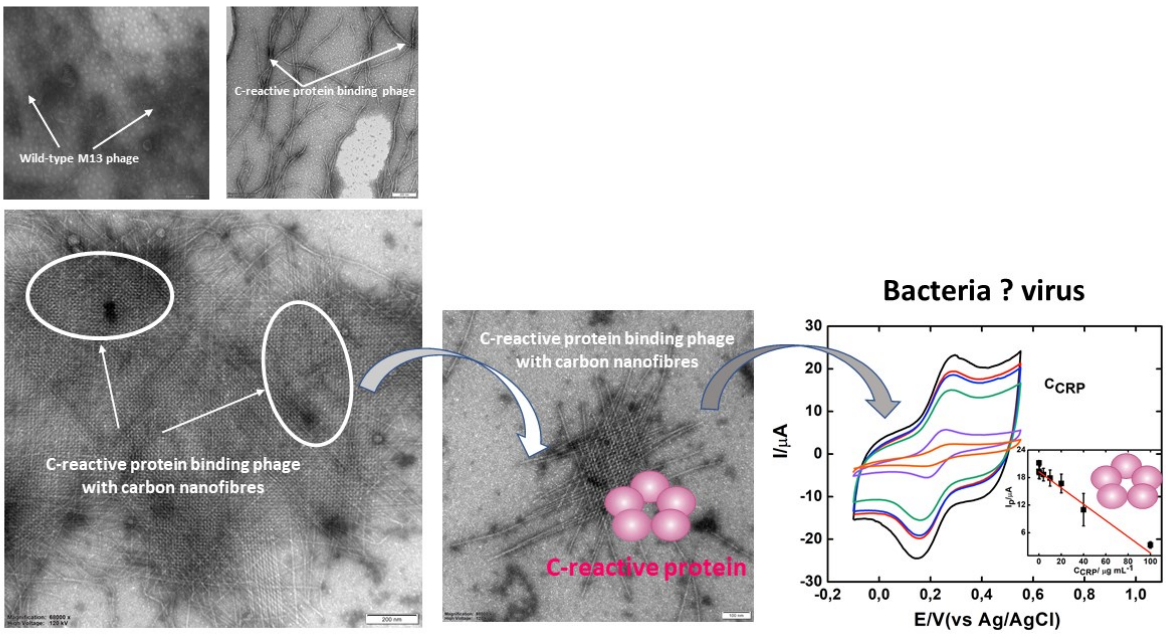

References

[1] M.A. Hemminga, W.L. Vos, P. V Nazarov, R.B.M. Koehorst, C.J.A.M. Wolfs, R.B. Spruijt, D. Stopar, Viruses: incredible nanomachines. New advances with filamentous phages, Eur. Biophys. J. 39 (2010) 541–550. doi:10.1007/s00249-009-0523-0.

[2] C. Shone, P. Wilton-Smith, N. Appleton, P. Hambleton, N. Modi, S. Gatley, J. Melling, Monoclonal antibody-based immunoassay for type A Clostridium botulinum toxin is comparable to the mouse bioassay., Appl. Environ. Microbiol. 50 (1985) 63 LP – 67. http://aem.asm.org/content/50/1/63.abstract.

[3] V.A. Petrenko, V.J. Vodyanoy, Phage display for detection of biological threat agents, J. Microbiol. Methods. 53 (2003) 253–262. doi:https://doi.org/10.1016/S0167-7012(03)00029-0.

[4] S. Pavan, F. Berti, Short peptides as biosensor transducers, Anal. Bioanal. Chem. 402 (2012) 3055–3070. doi:10.1007/s00216-011-5589-8.

[5] G.P. Smith, Filamentous fusion phage: novel expression vectors that display cloned antigens on the virion surface, Science (80-.). 228 (1985) 1315 LP – 1317. doi:10.1126/science.4001944.

[6] B. Bakhshinejad, S. Ghiasvand, Bacteriophages in the human gut: Our fellow travelers throughout life and potential biomarkers of heath or disease, Virus Res. 240 (2017) 47–55. doi:10.1016/j.virusres.2017.07.013.

[7] M. Łusiak-Szelachowska, B. Weber-Dąbrowska, E. Jończyk-Matysiak, R. Wojciechowska, A. Górski, Bacteriophages in the gastrointestinal tract and their implications, Gut Pathog. 9 (2017) 1–5. doi:10.1186/s13099-017-0196-7.

[8] O. Krut, I. Bekeredjian-Ding, Contribution of the Immune Response to Phage Therapy, J. Immunol. 200 (2018) 3037–3044. doi:10.4049/jimmunol.1701745.

[9] H. Xu, B. Cao, Y. Li, C. Mao, Phage nanofibers in nanomedicine: Biopanning for early diagnosis, targeted therapy, and proteomics analysis, Wiley Interdiscip. Rev. Nanomedicine Nanobiotechnology. (2020) 1–33. doi:10.1002/wnan.1623.

[10] J. Bábíčková, Ľ. Tóthová, P. Boor, P. Celec, In vivo phage display — A discovery tool in molecular biomedicine, Biotechnol. Adv. 31 (2013) 1247–1259. doi:https://doi.org/10.1016/j.biotechadv.2013.04.004.

[11] M. Trepel, W. Arap, R. Pasqualini, In vivo phage display and vascular heterogeneity: implications for targeted medicine, Curr. Opin. Chem. Biol. 6 (2002) 399–404. doi:https://doi.org/10.1016/S1367-5931(02)00336-8.

[12] R. Farr, D.S. Choi, S.-W. Lee, Phage-based nanomaterials for biomedical applications, Acta Biomater. 10 (2014) 1741–1750. doi:http://dx.doi.org/10.1016/j.actbio.2013.06.037.

[13] S.-W. Lee, A.M. Belcher, Virus-Based Fabrication of Micro- and Nanofibers Using Electrospinning, Nano Lett. 4 (2004) 387–390. doi:10.1021/nl034911t.

[14] A. Gutes, B.-Y. Lee, C. Carraro, W. Mickelson, S.-W. Lee, R. Mabouduan, Impedimetric graphene-based biosensors for the detection of polybrominated diphenyl ethers, Nanoscale. 5 (2013) 6048–6052. doi:10.1039/C3NR01268A.

[15] M. Janczuk, J. Niedziółka-Jönsson, K. Szot-Karpińska, Bacteriophages in electrochemistry: A review, J. Electroanal. Chem. 779 (2016) 207–219. doi:https://doi.org/10.1016/j.jelechem.2016.05.019.

[16] M. Janczuk-Richter, I. Marinović, J. Niedziółka-Jönsson, K. Szot-Karpińska, Recent applications of bacteriophage-based electrodes: A mini-review, Electrochem. Commun. 99 (2019) 11–15. doi:https://doi.org/10.1016/j.elecom.2018.12.011.

[17] K. Szot-Karpińska, A. Leśniewski, M. Jönsson-Niedziółka, F. Marken, J. Niedziółka-Jönsson, Electrodes modified with bacteriophages and carbon nanofibres for cysteine detection, Sensors Actuators B Chem. 287 (2019) 78–85. doi:https://doi.org/10.1016/j.snb.2019.01.148.

[18] K. Szot-Karpińska, P. Golec, A. Leśniewski, B. Pałys, F. Marken, J. Niedziółka-Jönsson, G. Węgrzyn, M. Łoś, Modified Filamentous Bacteriophage as a Scaffold for Carbon Nanofiber, Bioconjug. Chem. 27 (2016) 2900–2910. doi:10.1021/acs.bioconjchem.6b00555.

[19] L.-M.C. Yang, P.Y. Tam, B.J. Murray, T.M. McIntire, C.M. Overstreet, G.A. Weiss, R.M. Penner, Virus Electrodes for Universal Biodetection, Anal. Chem. 78 (2006) 3265–3270. doi:10.1021/ac052287u.

[20] V. Nanduri, I.B. Sorokulova, A.M. Samoylov, A.L. Simonian, V.A. Petrenko, V. Vodyanoy, Phage as a molecular recognition element in biosensors immobilized by physical adsorption, Biosens. Bioelectron. 22 (2007) 986–992. doi:https://doi.org/10.1016/j.bios.2006.03.025.

[21] H. Anany, Y. Chou, S. Cucic, R. Derda, S. Evoy, M.W. Griffiths, From Bits and Pieces to Whole Phage to Nanomachines: Pathogen Detection Using Bacteriophages, Annu. Rev. Food Sci. Technol. 8 (2017) 305–329. doi:10.1146/annurev-food-041715-033235.

[22] Ł. Richter, M. Janczuk-Richter, J. Niedziółka-Jönsson, J. Paczesny, R. Hołyst, Recent advances in bacteriophage-based methods for bacteria detection, Drug Discov. Today. 23 (2018) 448–455. doi:https://doi.org/10.1016/j.drudis.2017.11.007.

[23] L. Han, P. Liu, V.A. Petrenko, A. Liu, A Label-Free Electrochemical Impedance Cytosensor Based on Specific Peptide-Fused Phage Selected from Landscape Phage Library, Sci. Rep. 6 (2016) 22199. doi:10.1038/srep22199.

[24] J.P. Park, D.M. Cropek, S. Banta, High affinity peptides for the recognition of the heart disease biomarker troponin I identified using phage display, Biotechnol. Bioeng. 105 (2010) 678–686. doi:10.1002/bit.22597.

[25] J. Zhang, H. Spring, M. Schwab, Neuroblastoma tumor cell-binding peptides identified through random peptide phage display, Cancer Lett. 171 (2001) 153–164. doi:https://doi.org/10.1016/S0304-3835(01)00575-4.

[26] C. Gabay, I. Kushner, Acute-Phase Proteins and Other Systemic Responses to Inflammation, N. Engl. J. Med. 340 (1999) 448–454. doi:10.1056/NEJM199902113400607.

[27] I.M.R. Peter J. Delves, Seamus J. Martin, Dennis R. Burton, Roitt's Essential Immunology, John Wiley & Sons, Ltd, 2017.

[28] N.R. Sproston, J.J. Ashworth, Role of C-Reactive Protein at Sites of Inflammation and Infection, Front. Immunol. 9 (2018) 754. doi:10.3389/fimmu.2018.00754.

[29] D. Braig, T.L. Nero, H.-G. Koch, B. Kaiser, X. Wang, J.R. Thiele, C.J. Morton, J. Zeller, J. Kiefer, L.A. Potempa, N.A. Mellett, L.A. Miles, X.-J. Du, P.J. Meikle, M. Huber-Lang, G.B. Stark, M.W. Parker, K. Peter, S.U. Eisenhardt, Transitional changes in the CRP structure lead to the exposure of proinflammatory binding sites, Nat. Commun. 8 (2017) 14188. doi:10.1038/ncomms14188.

[30] A.K. Yagati, J.-C. Pyun, J. Min, S. Cho, Label-free and direct detection of C-reactive protein using reduced graphene oxide-nanoparticle hybrid impedimetric sensor, Bioelectrochemistry. 107 (2016) 37–44. doi:https://doi.org/10.1016/j.bioelechem.2015.10.002.

[31] J. Wang, J. Guo, J. Zhang, W. Zhang, Y. Zhang, RNA aptamer-based electrochemical aptasensor for C-reactive protein detection using functionalized silica microspheres as immunoprobes, Biosens. Bioelectron. 95 (2017) 100–105. doi:https://doi.org/10.1016/j.bios.2017.04.014.

[32] A. Johnson, Q. Song, P. Ko Ferrigno, P.R. Bueno, J.J. Davis, Sensitive Affimer and Antibody Based Impedimetric Label-Free Assays for C-Reactive Protein, Anal. Chem. 84 (2012) 6553–6560. doi:10.1021/ac300835b.

[33] C. Albrecht, P. Fechner, D. Honcharenko, L. Baltzer, G. Gauglitz, A new assay design for clinical diagnostics based on alternative recognition elements, Biosens. Bioelectron. 25 (2010) 2302–2308. doi:https://doi.org/10.1016/j.bios.2010.03.022.

[34] P.-C. Chou, J. Rick, T.-C. Chou, C-reactive protein thin-film molecularly imprinted polymers formed using a micro-contact approach, Anal. Chim. Acta. 542 (2005) 20–25. doi:https://doi.org/10.1016/j.aca.2004.12.074.

[35] X. Liu, W. Lin, P. Xiao, M. Yang, L.-P. Sun, Y. Zhang, W. Xue, B.-O. Guan, Polydopamine-based molecular imprinted optic microfiber sensor enhanced by template-mediated molecular rearrangement for ultra-sensitive C-reactive protein detection, Chem. Eng. J. 387 (2020) 124074. doi:https://doi.org/10.1016/j.cej.2020.124074.

[36] K.-W. Kim, B.-M. Kim, H.-W. Moon, S.-H. Lee, H.-R. Kim, Role of C-reactive protein in osteoclastogenesis in rheumatoid arthritis, Arthritis Res. Ther. 17 (2015) 41. doi:10.1186/s13075-015-0563-z.

[37] K. Chew, What's new in Emergencies Trauma and Shock? C-reactive protein as a potential clinical biomarker for influenza infection: More questions than answers, J. Emerg. Trauma. Shock. 5 (2012) 115–117. doi:10.4103/0974-2700.96477.

[38] R. Patel, Antimicrobial Restitance Keeps Me Up at Night, Microcosm. Fall (2019) 13.

[39] S.K. Vashist, A.G. Venkatesh, E. Marion Schneider, C. Beaudoin, P.B. Luppa, J.H.T. Luong, Bioanalytical advances in assays for C-reactive protein, Biotechnol. Adv. 34 (2016) 272–290. doi:https://doi.org/10.1016/j.biotechadv.2015.12.010.

[40] T. Ala-Kleme, P. Mäkinen, T. Ylinen, L. Väre, S. Kulmala, P. Ihalainen, J. Peltonen, Rapid Electrochemiluminoimmunoassay of Human C-Reactive Protein at Planar Disposable Oxide-Coated Silicon Electrodes, Anal. Chem. 78 (2006) 82–88. doi:10.1021/ac051157i.

[41] M. António, R. Ferreira, R. Vitorino, A.L. Daniel-da-Silva, A simple aptamer-based colorimetric assay for rapid detection of C-reactive protein using gold nanoparticles, Talanta. 214 (2020) 120868. doi:https://doi.org/10.1016/j.talanta.2020.120868.

[42] A.T.E. Vilian, W. Kim, B. Park, S.Y. Oh, T. Kim, Y.S. Huh, C.K. Hwangbo, Y.-K. Han, Efficient electron-mediated electrochemical biosensor of gold wire for the rapid detection of C-reactive protein: A predictive strategy for heart failure, Biosens. Bioelectron. 142 (2019) 111549. doi:https://doi.org/10.1016/j.bios.2019.111549.

[43] J.O. Koskinen, J. Vaarno, N.J. Meltola, J.T. Soini, P.E. Hänninen, J. Luotola, M.E. Waris, A.E. Soini, Fluorescent nanoparticles as labels for immunometric assay of C-reactive protein using two-photon excitation assay technology, Anal. Biochem. 328 (2004) 210–218. doi:https://doi.org/10.1016/j.ab.2004.02.029.

[44] M.H.F. Meyer, M. Hartmann, M. Keusgen, SPR-based immunosensor for the CRP detection—A new method to detect a well known protein, Biosens. Bioelectron. 21 (2006) 1987–1990. doi:https://doi.org/10.1016/j.bios.2005.09.010.

[45] I.N. Katis, P.J.W. He, R.W. Eason, C.L. Sones, Improved sensitivity and limit-of-detection of lateral flow devices using spatial constrictions of the flow-path, Biosens. Bioelectron. 113 (2018) 95–100. doi:https://doi.org/10.1016/j.bios.2018.05.001.

[46] N.-M.D. Courchesne, M.T. Klug, P.-Y. Chen, S.E. Kooi, D.S. Yun, N. Hong, N.X. Fang, A.M. Belcher, P.T. Hammond, Assembly of a Bacteriophage-Based Template for the Organization of Materials into Nanoporous Networks, Adv. Mater. 26 (2014) 3398–3404. doi:10.1002/adma.201305928.

[47] F. Marken, M.L. Gerrard, I.M. Mellor, R.J. Mortimer, C.E. Madden, S. Fletcher, K. Holt, J.S. Foord, R.H. Dahm, F. Page, Voltammetry at carbon nanofiber electrodes, Electrochem. Commun. 3 (2001) 177–180. doi:http://dx.doi.org/10.1016/S1388-2481(01)00132-1.

[48] G.P. Smith, V.A. Petrenko, Phage Display, Chem. Rev. 97 (1997) 391–410. doi:10.1021/cr960065d.

[49] R.K. Wilson, High-throughput purification of M13 templates for DNA sequencing, Biotechniques. 15 (1993) 414-416,418-420,422. http://europepmc.org/abstract/MED/8217153.

[50] K.J. Lee, J.H. Lee, H.K. Chung, E.J. Ju, S.Y. Song, S.Y. Jeong, E.K. Choi, Application of peptide displaying phage as a novel diagnostic probe for human lung adenocarcinoma, Amino Acids. 48 (2016) 1079–1086. doi:10.1007/s00726-015-2153-4.

[51] B.R. Putra, K. Szot-Karpińska, P. Kudła, H. Yin, J.A. Boswell, A.M. Squires, M.A. Da Silva, K.J. Edler, P.J. Fletcher, S.C. Parker, F. Marken, Bacteriophage M13 Aggregation on a Microhole Poly(ethylene terephthalate) Substrate Produces an Anionic Current Rectifier: Sensitivity toward Anionic versus Cationic Guests, ACS Appl. Bio Mater. 3 (2020) 512–521. doi:10.1021/acsabm.9b00952.

[52] G.T. Hess, J.J. Cragnolini, M.W. Popp, M.A. Allen, S.K. Dougan, E. Spooner, H.L. Ploegh, A.M. Belcher, C.P. Guimaraes, M13 Bacteriophage Display Framework That Allows Sortase-Mediated Modification of Surface-Accessible Phage Proteins, Bioconjug. Chem. 23 (2012) 1478–1487. doi:10.1021/bc300130z.

[53] J.C. Sanders, N.A.J. van Nuland, O. Edholm, M.A. Hemminga, Conformation and aggregation of M13 coat protein studied by molecular dynamics, Biophys. Chem. 41 (1991) 193–202. doi:http://dx.doi.org/10.1016/0301-4622(91)80019-N.

[54] Q. Yao, Y. Xiong, H. Wang, C. Wang, Q. Sun, MnO2 nanoflakes/cellulose nanofibre aerogel fabricated via ultrasonication for high-performance water desalination, J. Mater. Chem. A. 5 (2017) 9580–9590. doi:10.1039/C7TA01469D.

[55] S.J. Kerber, J.J. Bruckner, K. Wozniak, S. Seal, S. Hardcastle, T.L. Barr, The nature of hydrogen in x-ray photoelectron spectroscopy: General patterns from hydroxides to hydrogen bonding, J. Vac. Sci. Technol. A. 14 (1996) 1314–1320. doi:10.1116/1.579947.

[56] D.A. Marvin, R.D. Hale, C. Nave, M.H. Citterich, Molecular models and structural comparisons of native and mutant class I filamentous bacteriophages: Ff (fd, f1, M13), If1 and IKe, J. Mol. Biol. 235 (1994) 260–286. doi:https://doi.org/10.1016/S0022-2836(05)80032-4.

[57] P.-Y. Chen, R. Ladewski, R. Miller, X. Dang, J. Qi, F. Liau, A.M. Belcher, P.T. Hammond, Layer-by-layer assembled porous photoanodes for efficient electron collection in dye-sensitized solar cells, J. Mater. Chem. A. 1 (2013) 2217–2224. doi:10.1039/C2TA00771A.

[58] P.J. Yoo, K.T. Nam, A.M. Belcher, P.T. Hammond, Solvent-Assisted Patterning of Polyelectrolyte Multilayers and Selective Deposition of Virus Assemblies, Nano Lett. 8 (2008) 1081–1089. doi:10.1021/nl073079f.

[59] M. Graf, R.G. García, H. Wätzig, Protein adsorption in fused-silica and polyacrylamide-coated capillaries, Electrophoresis. 26 (2005) 2409–2417. doi:10.1002/elps.200410360.